Silica-alumina aerogels functionalized with amino-groups for the adsorption of CO2

The Journal of Supercritical Fluids 229 (2026) 106835

Contents lists available at ScienceDirect

The Journal of Supercritical Fluids

journal homepage: www.elsevier.com/locate/supflu

Silica-alumina aerogels functionalized with amino-groups for the adsorption of CO_2

Marta Gallo *, Marco Armandi, Fabiana Mangano, Silvia Ronchetti, Mauro Banchero, Luigi Manna

Dipartimento di Scienza Applicata e Tecnologia, Politecnico di Torino, Corso Duca Degli Abruzzi, 24, Torino 10129, Italy

HIGHLIGHTS

- silica-alumina aerogels with amino groups were prepared through a one-pot process.
- low amine-content did not confer significantly different properties.
- high amine-content significantly improved CO_2 adsorbed amount and selectivity over N_2.

GRAPHICAL ABSTRACT

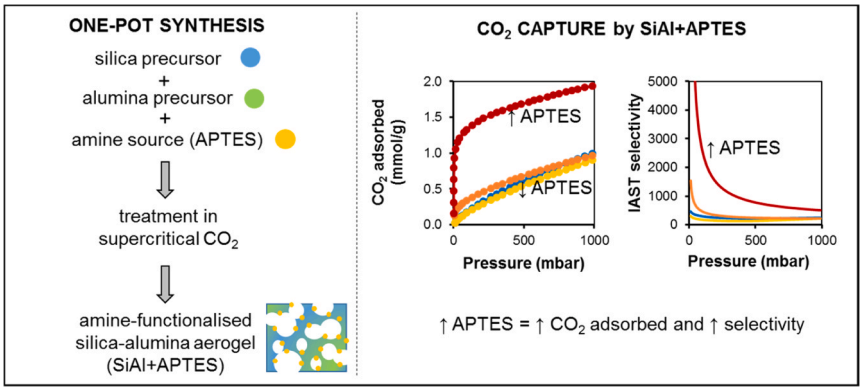

ARTICLE INFO

Keywords:
Silica-alumina aerogel
APTES-functionalization
CO_2 capture
One-pot synthesis

ABSTRACT

To overcome climate challenges, emerging CO_2 capture technologies focus on innovative solid sorbents, like aerogels. Silica aerogels, in particular, have emerged as an exceptional class of materials with unique properties even though their adsorption selectivity towards CO_2, and their thermal and mechanical properties are limited. In this research, a hybrid silica-alumina aerogel has been prepared, to merge the elevated surface area typical of silica with the basic character (favorable to CO_2 adsorption) and the high thermal and mechanical resistance typical of alumina. For the first time, these silica-alumina aerogels were functionalized with 3-aminopropyltriethoxysilane (APTES) amino groups through a one-pot process. This approach was chosen to directly introduce functional groups during gel formation, reducing the number of post-synthesis steps. The functionalization with amino groups aims to strengthen the interactions with CO_2 molecules via acid–base interactions, thus enhancing adsorption capacity and selectivity. Three samples with increasing APTES content as well as a reference without any functionalization were prepared and characterized in terms of physico-chemical and adsorption properties. The results of CO_2 and N_2 adsorption tests as well as *in situ* FTIR suggest that low functionalization does not confer a significant advantage in CO_2 capture. Higher APTES contents, instead, lead to a significant increase in the total quantity of adsorbed CO_2 and in higher selectivity over N_2 (calculated according to the Ideal Adsorbed

* Corresponding author.
E-mail address: marta.gallo@polito.it (M. Gallo).

https://doi.org/10.1016/j.supflu.2025.106835
Received 6 August 2025; Received in revised form 5 November 2025; Accepted 7 November 2025
Available online 8 November 2025

Solution Theory). Moreover, also the strength of interaction increases, since not only physisorption, but also chemisorption takes place.

1. Introduction

Climate change stands as one of the most formidable challenges confronting human society in the 21st century. The constantly increasing concentration of greenhouse gases attributed to human activities, such as fossil fuel combustion and deforestation, is identified as a key driver of the global temperature rise. Carbon dioxide (CO_2), which constitutes approximately 60 % of greenhouse gases emissions, primarily arises from the combustion of fossil fuels and is acknowledged as the principal responsible for global warming [1]. To mitigate the adverse effects of CO_2 emissions, there is an urgent need for innovative and efficient technologies for its capture and storage. There are three primary methods for CO_2 capture: pre-combustion, post-combustion, and oxycombustion. These methods entail various processes for separating CO_2 from gas mixtures, including absorption, physical/chemical adsorption, membrane separation, and cryogenic separation. However, challenges exist with all these technologies, including their high-energy consumption, corrosion risks to equipment, degradation of amines used in liquid phase absorption, potential generation of toxic by-products, and excessive solvent loss through evaporation [2]. To overcome these drawbacks, emerging CO_2 capture technologies currently focus on solid physical and chemical adsorbents, such as zeolites, metal-organic frameworks, activated carbon, mesoporous silica, and aerogels. Among these, silica aerogels, exhibiting a combination of high surface area, low density, and tunable porosity, are highly attractive for the development of next-generation CO_2 adsorbents [3–5]. Although silica aerogels are good adsorbents, owing to the intrinsic inertness of the surface Si-OH groups, their adsorption capacity and selectivity towards CO_2 are limited. The CO_2 capture capacity, however, can be improved by functionalizing the matrix with amino groups [6,7]. In fact, the inherent basic properties of amines play a pivotal role in facilitating the absorption of a significant amount of CO_2. Indeed, in the work by Cui et al. [8] the adsorption capacity of silica aerogel modified with 3-aminopropyltriethoxysilane (APTES) reached ~2.3 mmol/g and was proved to be roughly 5 times higher than that of pure silica aerogel. Similarly, Choi and coworkers functionalized silica aerogel with increasing amounts of APTES, passing from a CO_2 adsorption of 0.1 mmol/g for the pristine silica aerogel to 3.1 mmol/g for the aerogel with a high APTES content (APTES/silica ratio equal to 2.5) [9]. Therefore, in this work we focused on functionalizing a silica-based aerogel with amino groups derived from APTES. In addition, we chose to functionalize silica-alumina aerogels, rather than pure silica aerogels, to merge the high surface area of silica, with the high thermal and mechanical resistance of alumina [7] as well as its basic character, which may be favorable to CO_2 capture [10]. Commonly, amino-modified silica aerogels are obtained either by bonding amines to the surface of the support through strong chemical bonds (i.e. grafting [11]) or by impregnating the amine within the pore volume by weak physical interactions (i.e. wet impregnation [12]). In general, amine-grafted sorbents are more stable and withstand adsorption-desorption cycle better. Amine-impregnated materials, instead, usually have a higher CO_2 capture capacity [13]. Both techniques, however, require at least an additional step after the aerogel synthesis, imply the use of organic solvents and, often, involve thermal treatments. In this work, silica-alumina hybrid aerogels were synthesized with an acid-base sol-gel procedure adapted from Tamon and coworkers [14]. Amino-groups were introduced directly during the aerogel synthesis with a simple co-precursor sol-gel procedure (inspired by [6]), without recurring to a subsequent grafting step [15]. The so-obtained gels were dried in supercritical CO_2, to obtain monolithic aerogels. To the authors' knowledge, this type of material has been synthesized for the first time during this research and there are no precedents in the literature. In total, three types of silica-alumina aerogels functionalized with increasing contents of APTES were obtained. A silica-alumina sample without APTES was also synthesized as a reference. All samples were characterized in terms of physico-chemical properties as well as CO_2 capture ability.

2. Materials and methods

2.1. Reagents

The following reagents were used as received: aluminum tri sec-butoxide (ATBS, $Al[OCH(CH_3)C_2H_5]_3$, Thermo Scientific), tetramethyl orthosilicate (TMOS, $Si(OCH_3)_4$, Fluka), 2-butanol ($C_4H_{10}O$, Emplura-Supelco), (3-aminopropyl)triethoxysilane (APTES, $C_9H_{23}NO_3Si$), anhydrous ethanol (C_2H_6O, Carlo Erba). Ammonium hydroxide (NH_4OH, Sigma Aldrich), and hydrochloric acid (HCl, Sigma Aldrich) were diluted with ultrapure water to obtain the desired concentration.

2.2. Preparation of the gels

The synthesis of the silica-alumina aerogel (hereafter called "SiAl") was inspired by [14]. The molar ratios chosen to calculate the amount of the reagents are reported in Table 1. In a typical synthesis, first, solution A was prepared mixing 4.57 g of TMOS, 0.63 g of HCl solution (0.01 M), and 11.55 g of 2-butanol for 1.5 h (200 rpm, T_{amb}). Second, solution B was obtained mixing 3.30 g of 2-butanol, and 0.87 g of ATSB for 5 min (200 rpm, T_{amb}). After, solutions A and B were mixed at 80 °C for 2 h. In the end, 4.81 g of NH_4OH solution (1.0 M) were added; after a couple of minutes the stirring was stopped, the solution was poured into a beaker containing cylindrical glass moulds and it was kept at 80 °C until it turned into a gel (within a few minutes) (Figure S.1). Once the samples of gel (alcogel) were ready, they were covered with ethanol and aged for 7 days at ambient temperature.

Three types of silica-alumina aerogels functionalized with APTES (named "SiAl+APTES") were prepared by varying the number of APTES moles added during the synthesis. In particular, 2.5 mmol, 7.5 mmol, and 22.5 mmol of APTES were introduced, keeping the amount of TMOS constant and equal to 30 mmol. The resulting samples are called SiAl+APTES_2.5, SiAl+APTES_7.5, and SiAl+APTES_22.5, respectively.

To synthesize the SiAl+APTES samples, solutions A and B were prepared as previously explained; they were mixed and then, APTES and water were immediately added. The amounts of APTES and water were 0.57 g and 0.57 g, respectively, for SiAl+APTES_2.5, 1.68 g and 0.85 g for SiAl+APTES_7.5, and 5.00 g and 1.70 g for SiAl+APTES_22.5. The solution was mixed for 1 h (200 rpm, T_{amb}) before adding 4.81 g of NH_4OH, then it was again mixed for 2 min. Finally, the solution was poured into cylindrical glass moulds and left to gel at ambient temperature; gelation occurred in 1.5 h. The alcogels were covered with ethanol and aged for 7 days at ambient temperature.

2.3. Aerogel production using supercritical drying

The alcogel samples were dried by means of a supercritical drying process using carbon dioxide (CO_2). A simplified schematic diagram of the apparatus used is shown in Fig. 1.

Liquid CO_2 from a dip-tube cylinder was precooled to prevent cavitation and pressurized using a dual-piston pump. The fluid then passed through a heating coil, a high-pressure vessel containing the samples, and an automated back-pressure regulator (ABPR). Both the heating coil and the vessel were housed inside a thermostatically controlled oven.

The vessel was a stainless-steel cylinder (internal diameter 1.4 cm,

length 22 cm; internal volume ~34 cm^3) arranged horizontally. Inside, the samples were separated by layers of glass wool. Each sample consisted of a small glass cylinder (internal diameter 8 mm, length 20 mm) containing the previously formed alcogel. A total of 6 samples were dried simultaneously.

At the initial stage, liquid CO_2 entered the vessel at 25.0 °C, while the ABPR valve remained fully closed. Once the operating pressure of 105 bar was reached, the ABPR was activated to maintain constant pressure. The system was then gradually heated to the drying temperature (40.0 °C). Under these conditions (40.0 °C and 105 bar), CO_2 became supercritical. The process continued with a steady flow of supercritical CO_2 at 4.0 g•min^{-1} for at least 4 h, which was sufficient to fully replace the ethanol within the gel. The total CO_2 consumption for the entire process was approximately 1.4 kg.

At the end, the CO_2 supply was stopped and the system was depressurized at approximately 2.5 bar•min^{-1}while maintaining the drying temperature, to prevent structural damage to the samples. Once atmospheric pressure was reached, the vessel was allowed to cool to room temperature and the dried samples were removed.

2.4. Characterization of the aerogels

The aerogels were weighted, measured, and analyzed as follows. Fourier Transformed Infra-Red Spectroscopy (FTIR) spectra were recorded in transmission mode using a Bruker Tensor 27 spectrometer (Bruker, Billerica, MA, USA) equipped with a liquid nitrogen-cooled mercury–cadmium–telluride (MCT) detector, operating at 2 cm^{-1} resolution. The samples, in powder form, were pressed into thin self-supporting wafers and outgassed under vacuum (residual pressure ≈ 1•10^{-4} mbar).

For X-ray Photoelectron Spectroscopy analyses (XPS), a VersaProbe 5000 by Physical Electronic instrument, with a monochromatic radiation source Al K_α 1486.6 eV, was employed.

Thermogravimetric analyses (TGA) were carried out using a Setaram TGA (Caluire, France) by heating the samples between 20 °C and 800 °C with a heating rate of 10 °C min^{-1} in air flow.

X-Ray Diffraction (XRD) data were obtained through a Panalytical Empyrean instrument (Cu Kα radiation, Malvern Panalytical, Almelo, The Netherlands) operating at 40 kV and 40 mA, equipped with a solid-state detector (PIXcel1D). The measurements were conducted within a wide-angle range (5° to 60°).

Nitrogen adsorption-desorption isotherms were acquired using an ASAP 2020 Plus analyzer (Micromeritics, Norcross, GA, USA). Samples were outgassed at 70 °C for 3 h until the residual pressure was < 10 μmHg. The surface area was calculated using the Brunauer–Emmett–Teller (BET) method [16], while the pore volume was obtained using the Barrett–Joyner–Halenda (BJH) method [17], using desorption isothermal data.

Isothermal adsorption of CO_2 was evaluated with the same instrument used to acquire the nitrogen isotherms; in this case, samples were outgassed at 120 °C for 2 h. To verify the possible presence of irreversibly adsorbed CO_2, two-run experiments were conducted at 25 °C. After the first adsorption run, the samples were outgassed at room temperature (for 1 h) and subsequently underwent a second adsorption run, in which only reversible physisorption occurs.

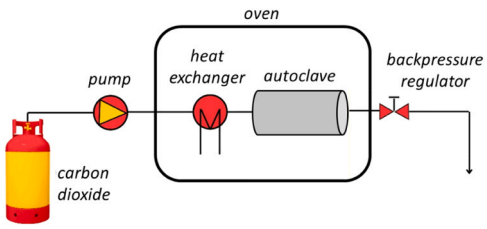

Fig. 1. Scheme of the experimental apparatus employed for the supercritical drying.

The same instrument and procedure were used to measure N_2 adsorption isotherms at 25 °C, which were employed to investigate gas adsorption selectivity according to the Ideal Adsorption Solution Theory (IAST) [18–20]. The CO_2/N_2 adsorption selectivity at 25 °C was calculated with IAST, for a mixture composition with a CO_2:N_2 ratio equal to 15:85, considering that flue gases typically contain larger amounts of N_2 than CO_2 [21]. The adsorption selectivity is given by Eq. 1:

$$IAST\ Selectivity = \frac{qCO_2/qN_2}{pCO_2/pN_2} \quad (1)$$

Where q represents the mole fractions of the components in the adsorbed phase, while p refers to the bulk phase.

In situ FTIR analyses were performed exposing the samples at different CO_2 equilibrium pressures at room temperature. Thermal pre-treatment and CO_2 dosage were carried out using a standard vacuum frame, in an IR cell equipped with KBr windows. For IR measurements, the powders were pressed into thin self-supporting wafers (ca. 8 mg•cm^{-2}) and outgassed under vacuum (residual pressure ≈ 1•10^{-4} mbar) at 120 °C for 2 h, as described elsewhere [22]. IR spectra were recorded after dosing CO_2 (purity 5.5•10^{-3} to 112.5 Torr equilibrium pressure range) at room temperature on the pre-treated samples. The IR spectra were normalized to the wafer density. Difference spectra were obtained by subtracting the spectrum of the bare wafer (before CO_2 adsorption). After CO_2 adsorption, an evacuation step (30 min) at room temperature was performed to check the reversibility of the interaction.

3. Results

The composition of the silica-alumina aerogels was studied by FTIR analysis (Fig. 2). In all samples, the broad band between 3200 cm^{-1} and 3700 cm^{-1} is attributable to –OH groups, which can be either due to silica (silanols) or to alumina [23]. The peaks around 2900 cm^{-1} can be ascribed to the stretching of -CH groups of organic components [24]; these can be either due to the alkyl chain of APTES (in functionaed samples) or to precursor molecules not completely hydrolysed. The peaks observed around 1400 cm^{-1} are likely connected to the presence of organic components too, as they can be ascribed to the bending of -CH groups (1450 cm^{-1} to 1470 cm^{-1}, [24]). It is worth mentioning that also C-N bond may adsorb in a similar wavenumber range (1440 cm^{-1} to 1460 cm^{-1} [25], [26]); this would indicate the presence of some N also in the SiAl sample (likely due to impurities probably related to the NH_4OH reagent). As reported in the literature, a signal related to Al-OH is identifiable around 1640 cm^{-1} [23], [27]. In the functionalized

Table 1
Molar ratios of reagents used for the synthesis of the different samples.

Sample	ATSB	TMOS	TMOS + ATSB	NH_4OH sol 1.0 M	HCl sol 0.01 M	2 – butanol**	APTES	total H_2O*
SiAl	0.1	0.9	1	8	0.9	6	-	8.9
SiAl+APTES_2.5 mmol	0.1	0.9	1	8	0.9	6	0.075	10
SiAl+APTES_7.5 mmol	0.1	0.9	1	8	0.9	6	0.225	10.5
SiAl+APTES_22.5 mmol	0.1	0.9	1	8	0.9	6	0.675	11.9

*This value represents the sum of moles of the water in ammonia solution, HCl solution, and of the water added with APTES
**Considering in total 6 moles of 2-butanol, 4.7 moles are used for solution A and 1.3 moles for solution B.

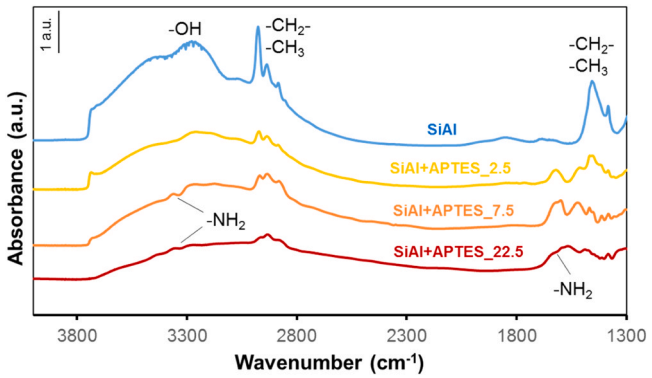

Fig. 2. FTIR spectra of the samples with (SiAl+APTES) and without functionalization (SiAl).

samples, the weak peak around 3300 cm^{-1} and the peaks centered at 1600 cm^{-1} are attributed to the -NH_2 stretching and bending mode, respectively [24].

The surface composition of the aerogels was analysed through XPS surveys; the results are reported in Table 2. No clear trend is observed for O and Al. A significant presence of C is detected in the SiAl aerogel, in accordance with the signal of organic components observed by FTIR. Interestingly, the percentage of C in the functionalized samples increases with the APTES content, since the APTES molecules contain alkyl chains. The Si content, on the opposite, decreases when the APTES content is increased, so suggesting that the functionalization influences the silica network formation. Unexpectedly, a small percentage of N is detected in the SiAl sample (likely due to the NH_4OH synthesis catalyst), in accordance with the FTIR spectra, whose peak around 1440 cm^{-1} to 1460 cm^{-1} may be related to C-N bond. In the functionalized aerogels, the content of N increases with the APTES content. It is worth noting that in the samples with the lowest APTES content (SiAl+APTES_2.5 and SiAL+APTES_7.5), the N peak is observed mainly at 401.7 eV, which belongs to protonated N [28,29] (Fig. 2A). However, in the SiAl+APTES_22.5, the main N peak is located at 399.6 eV, indicating the presence of deprotonated N (Fig. 3A). Finally, Al is detected in all samples at 75 eV [30] (Fig. 3B) even though its presence is limited and included between 1.0 and 3.1 at%.

The results of thermogravimetric analyses and the first derivative of mass loss versus temperature (dTG) are reported in Fig. 4A-B and Table 3. Mass losses that occur before 150 °C (whose dTG peak is around 70 °C to 100 °C, Fig. 4B) can be ascribed to the evaporation of physisorbed water. It is observed that all the functionalized samples lose significantly less physisorbed water than the sample as such, meaning that their surface is more hydrophobic. This is coherent with the introduction of alkyl chains (of APTES) on the sample surface; alkyl chains, in fact, being non-polar, are hydrophobic [32]. In the non-functionalized SiAl aerogel, the mass loss observed between 150 °C and 800 °C is considerably higher than that ascribable to the sole condensation of the silanols, which typically occurs at these temperatures [33]. This mass loss can be attributed to the degradation of residual organic components from the synthesis process, in agreement with what was observed with the FTIR analyses. This is also coherent with the dTG peak observed around 200 °C in the SiAl sample (Fig. 4B), which can be ascribed to the degradation of organic components [34]. In the functionalized samples, the mass loss between 150 °C and 800 °C, may be due the degradation of residues of precursors (as observed in the non-functionalized SiAl aerogels) and/or to the amines introduced during the synthesis. The derivative of the mass loss does not present significant peaks around 200 °C (Fig. 4B), suggesting that the residual organic components are limited in the functionalized samples. Several peaks are observed above 250 °C (Fig. 4B): these are compatible with the degradation temperature of grafted APTES [35], confirming the successful incorporation of APTES in the materials. Interestingly, these peaks are more visible in the samples with the highest APTES content. However, since the contributions of amines and organic residues cannot be separated (as the degradation temperatures fall in the same range) it is not possible to deduce the exact mass content of amines from this measurement. In general, in the functionalized samples the total mass loss is lower than that observed in the sample as such and increases with the APTES content.

Table 2
Atomic composition of samples according to XPS surveys (error on atomic percentages from XPS surveys are of ≈5 % for O, C, and Si and up to 30 % for N and Al [31]).

Sample	O (at%)	C (at%)	Si (at%)	N (at%)	Al (at%)
SiAl	52.1	26.6	18.4	1.5	1.0
SiAl+APTES_2.5	57.3	19.3	19.2	2.4	1.9
SiAl+APTES_7.5	51.7	23.7	16.7	4.7	3.1
SiAl+APTES_22.5	42.9	32.1	16.3	7.5	1.2

XRD patterns at wide angles (Fig. 5) present only a halo, typical of amorphous silica [36,37], confirming the absence of crystalline phases, such as alumina.

The N_2 adsorption isotherm curves are reported in Fig. 6A. All samples present a type IV curve with a H1 hysteresis loop according to the IUPAC classification [38]. This is typical of mesoporous materials with uniform porosities and in a narrow range [38,39]. The specific surface area ranges from 530 m^2/g for the SiAl+APTES_22.5 sample to 870 m^2/g and 880 m^2/g for the non-functionalized SiAl aerogel and the SiAl+PATES_7.5 sample (Table 4). The porous volume varies between 1.2 cm^3/g for SiAl+APSTE_22.5 and 3.0 cm^3/g for SiAl. For the non-functionalized SiAl aerogel, the pore size distribution is single-mode, and with a maximum around 15.2 nm (Fig. 6B). For the functionalized samples, instead, the pore distribution is larger, with an average value ranging between 15 nm and 20 nm (Table 4). The loss of homogeneity of pore size in the functionalized samples may be justified by the introduction of APTES during the sol-gel synthesis. The APTES molecules, interacting with the silica and alumina precursors, likely affect the silica-alumina network, altering its order.

Table 4 reports also an estimation of the average apparent density obtained by dividing the mass of the specimens by their volume (calculated geometrically). The results vary between 0.12 g/cm^3 and 0.30 g/cm^3, without any clear correlation with the APTES content. Finally, the average volume shrinkage induced by supercritical drying (Table 4) seems to decrease with increasing APTES content, suggesting that the final aerogel properties are a result of the combined influence of supercritical drying and APTES concentration.

CO_2 adsorption isotherms were measured on all samples (at 25 °C). To verify the possible presence of irreversibly adsorbed CO_2, two-run experiments were conducted. After the first adsorption run, the samples were outgassed at room temperature (for 1 h) and subsequently underwent a second run, in which only reversible physisorption occurs. The reference sample, the non-functionalized SiAl aerogel, adsorbs a maximum amount of 0.99 mmol of CO_2 per gram of material at 1 bar and does not present any sign of irreversibility (the two runs are overlapped) (Fig. 7A). The SiAl+APTES_2.5 sample does not present any irreversible phenomenon either and adsorbs 0.90 mmol/g (Fig. 7B). SiAl+APTES_7.5 adsorbs a similar amount of CO_2 (0.96 mmol/g), but a minority of the adsorption phenomena is irreversible (at room temperature) as run 2 does not overlap with run 1 but shows slightly lower values (Fig. 7C). Finally, the SiAl+APTES_22.5 sample absorbs a significantly higher quantity of CO_2 (1.94 mmol/g), but with non-negligible irreversible phenomena (run 2 reaches a maximum amount of 1.58 mmol/g) (Fig. 7D).

To better compare the performance of the different adsorbents, run 1 of all samples are gathered in Fig. 8. SiAl+APTES_2.5 presents a behaviour comparable to that of the non-functionalized sample, SiAl. Although SiAl, SiAl+APTES_2.5, and SiAl+APTES_7.5 adsorb roughly the same total amount of CO_2, at lower pressures SiAl+APTES_7.5

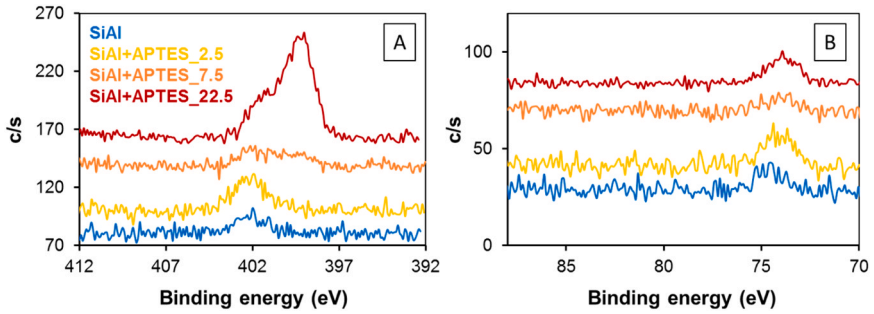

Fig. 3. High-resolution XPS spectra of N (A) and Al (B) of the samples with (SiAl+APTES) and without functionalization (SiAl).

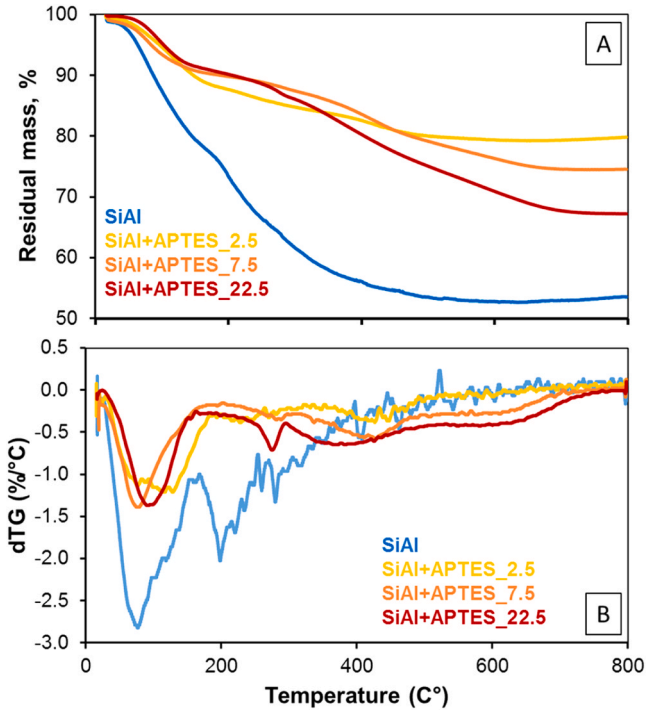

Fig. 4. TGA (A) and dTG (B) of the samples with (SiAl+APTES) and without functionalization (SiAl).

Table 3
Mass losses detected by TGA.

Sample	Mass loss < 150 °C (%)	Mass loss 150 °C to 800 °C (%)
SiAl	21	46
SiAl+APTES_2.5	10	20
SiAl+APTES_7.5	9	25
SiAl+APTES_22.5	9	33

exhibits a downward concavity, whereas the curves of the other two samples follow a linear trajectory. This reveals a higher affinity between SiAl+APTES_7.5 and CO_2 at low pressure. The downward concavity is significantly accentuated in SiAl+APTES_22.5, where about 70 % of the total adsorbed CO_2 is adsorbed at pressure lower than 100 mbar.

To better assess the interaction between the samples surface and CO_2, *in situ* FTIR was employed. The spectra were acquired at increasing CO_2 equilibrium pressure; the difference spectra, which were obtained by subtracting to each spectrum the one recorded prior to CO_2 adsorption, are reported in Fig. 9. For the SiAl and SiAl+APTES_2.5 samples (Figs. 9A-B and 9C-D, respectively), only one peak appears at around 2340 cm^{-1}, which increases at higher CO_2 pressures. This peak can be attributed to molecular physisorbed CO_2 [40], and it totally disappears

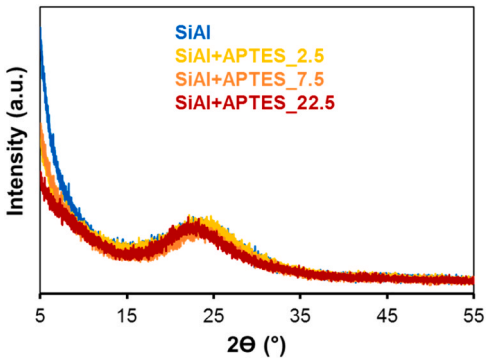

Fig. 5. X-ray diffraction patterns at wide angles of the samples with (SiAl+APTES) and without functionalization (SiAl).

after the outgassing step (dashed line in Fig. 9A-C), so indicating that the adsorption phenomenon is completely reversible. For SiAl+APTES_7.5 and SiAl+APTES_22.5, new bands appear around 1500 cm^{-1} to 1600 cm^{-1} (Figs. 9F and 9H), indicating the formation of carbamates [41–43] caused by the chemical interaction between APTES and CO_2. Interestingly, in SiAl+APTES_22.5 the peak of gaseous CO_2 rather than that of molecular physisorbed CO_2 is observed at around 2340 cm^{-1} (Fig. 9G). This suggests that in this sample CO_2 interacts first with the amine sites through chemisorption forming carbamates; only when the amine sites are saturated, CO_2 is observed in gaseous form (without physisorption phenomena). Although weak, the band of carbamates is still visible after the outgassing step both in SiAl+APTES_7.5 and SiAl+APTES_22.5 samples (Fig. 9F-H).

For practical applications such as CO_2 capture from flue gas, selective adsorption of CO_2 over N_2 is highly desirable. The Ideal Adsorption Solution Theory is a simple and widely used technique [44] to predict CO_2/N_2 selectivity based on the single-component gas adsorption results [19,44]. Thus, N_2 adsorption isotherms at 25 °C were measured (Fig. 10A) and the IAST selectivity for a 0.15/0.85 CO_2/N_2 molar mixture was calculated (Fig. 10B).

For all materials, both functionalized and non-functionalized, the amount of N_2 adsorbed was very low (below 0.03 mmol/g). For selected pressures, the ratio between the adsorbed amounts of CO_2 and N_2 was calculated and adjusted by multiplying by 0.85/0.15 (Eq.1), in order to mimic the typical flue gas composition (CO_2:N_2 = 15:85). The resulting values of IAST selectivity are reported in Fig. 10B. Among all tested samples, SiAl+APTES_22.5 shows a significantly higher CO_2/N_2 selectivity over the entire pressure range, likely due to its surface functionalization.

4. Discussion

After supercritical CO_2 drying, monolithic aerogels containing silica, alumina, and functionalized with APTES were successfully obtained

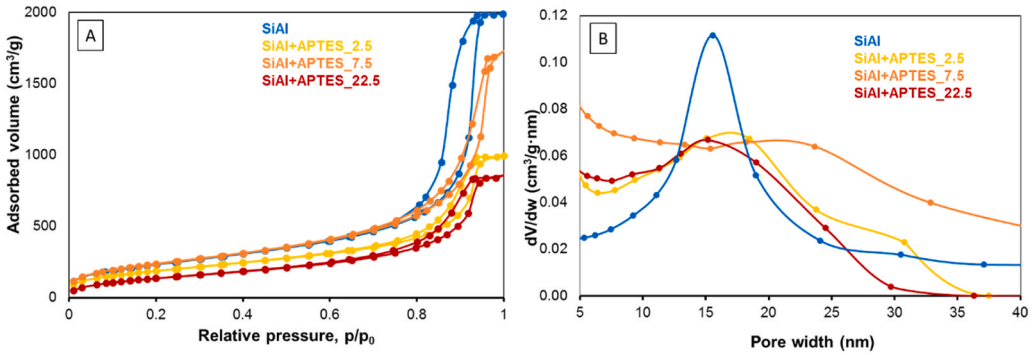

Fig. 6. Nitrogen adsorption isotherms (A) and pore size distribution according to the BJH model (B) of the samples with (SiAl+APTES) and without functionalization (SiAl).

Table 4
Textural properties, average apparent density, and average volume shrinkage upon drying of the samples with (SiAl+APTES) and without functionalization (SiAl) (std = standard deviation).

Sample	Specific surface area (m^2/g)	Pore volume (cm^3/g)	Average pore diameter (nm)	Apparent density ± std (g/cm^3)	Average volume shrinkage ± std (%)
SiAl	870	3.0	15.6	0.16 ± 0.02	36 ± 3
SiAl+APTES_2.5	700	1.5	16.0	0.30 ± 0.05	40 ± 4
SiAl+APTES_7.5	880	2.5	20.4	0.12 ± 0.04	30 ± 9
SiAl+APTES_22.5	530	1.2	15.0	0.19 ± 0.02	27 ± 8

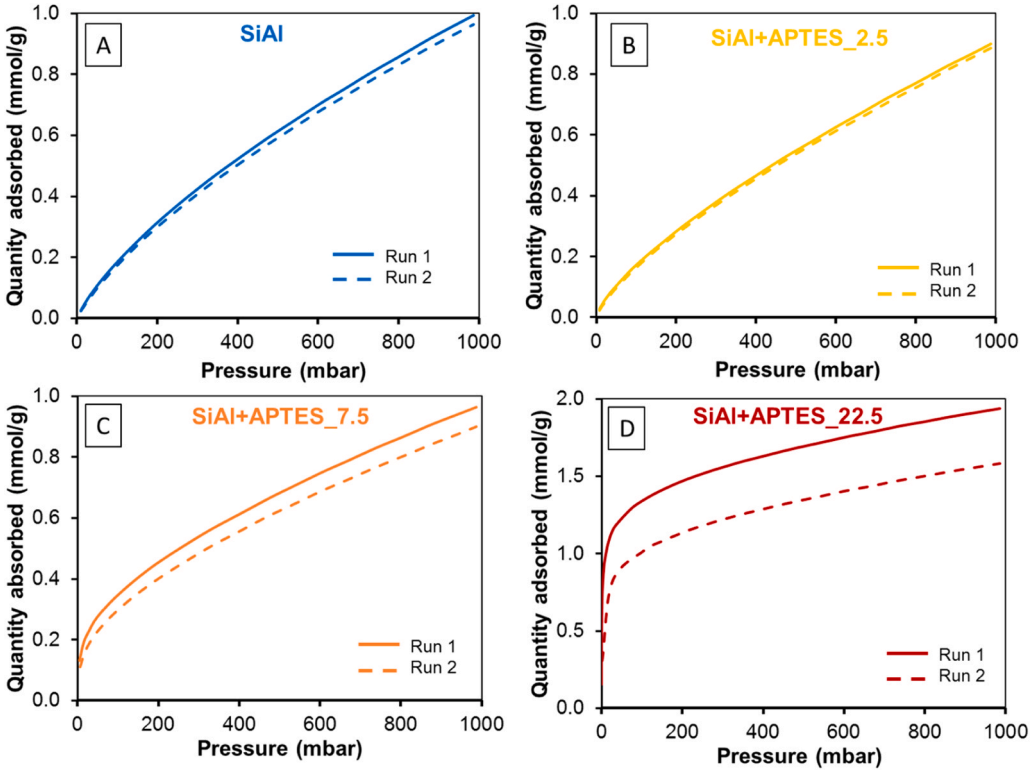

Fig. 7. CO_2 adsorption isotherms at 25 °C of the samples without (SiAl, A) and with functionalization (SiAl+APTES, B-C-D).

(Figure S.1). FTIR and XPS analyses (Figs. 2 and 3B), in fact, confirm the presence of organic components (alkyl chains) and of nitrogen, which may be ascribed to the incorporation of APTES. The synthesis process was adapted to introduce the APTES molecules directly during the aerogel formation through a one-pot procedure, reducing the number of post-synthesis steps. To the authors' knowledge, this is the first time that such a synthesis procedure is reported.

FTIR analyses underline the presence of organic moieties in all samples (including that without APTES, SiAl), suggesting that some of the precursor molecules (most probably ATSB) has not been completely hydrolysed during the synthesis. This phenomenon is also reported in the literature for similar precursors during the formation of titania aerogels [14]. This hypothesis is also supported by the high resolution XPS spectra of C (Figure S.2). A secondary component is observed

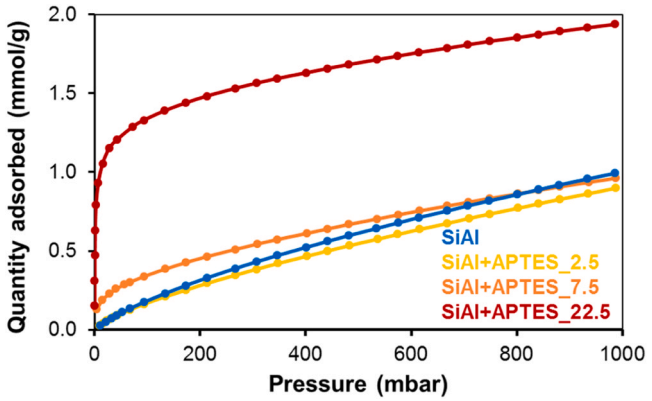

Fig. 8. Comparison of the CO_2 adsorption isotherms at 25 °C of the samples.

around 288 eV for the SiAl sample (arrow in Figure S.2). This signal is consistent with C-O and C═O bonds [44,45], which may arise from non-hydrolyzed precursors. Among the APTES-functionalized samples, this component is only visible for the material with the lowest APTES content, while it completely disappears in SiAl+APTES_7.5 and SiAl+APTES_22.5. The presence of organic residues is coherent with the significant mass loss registered above 150 °C by ATG in the SiAl sample (Fig. 4A) and the peak observed around 200 °C by dTG (Fig. 4B). Interestingly, the mass loss registered by ATG between 150 °C and 800 °C in the functionalized samples is lower than that observed in the sample as such (Fig. 4A) and no significant peaks are observed by dTG around 200 °C (Fig. 4B), suggesting that the organic content is lower in the samples with APTES. This result may be justified by the fact that in the samples with APTES, the time lapse between the addition of H_2O and gelation is longer than in the SiAl sample, thus allowing a more complete hydrolysis of the precursor molecules to be obtained (consistently with what observed by FTIR). Indeed, a possible strategy to reduce the amount of organic residues may consist in adding the majority of H_2O at the very beginning of the synthesis process (without changing the molar ratios), to increase the time available for the hydrolysis of the precursors. Experiments in this sense are currently ongoing; however, the presence of organic residues may not be detrimental to the adsorption capacities of the samples.

The presence of organic residues unfortunately prevented an accurate quantification of the amine content from TGA analysis. Nevertheless, an estimation can be obtained from the XPS results (Table 2). Using the data as collected, the amine content can be calculated as reported in the first column of Table 5 (expressed as mmol of amine per gram of silica). Assuming that the nitrogen detected in the SiAl sample is constant and not related to amine groups (but rather to the reagent NH_4OH), a "corrected" nitrogen amount can be calculated by subtracting the N content of SiAl from that of the functionalized samples. In this way, a lower amine content is obtained, as shown in the second column of Table 5. Finally, the theoretical amine loading, based on the amount of reagents used, is reported in the third column of Table 5.

When comparing these values, the theoretical content for SiAl+APTES_2.5 and SiAl+APTES_7.5 falls between the two estimates derived from the XPS data. This suggests that nitrogen contamination is present in all samples, leading to an overestimation of the amine content when raw XPS data are used. However, since the N contamination is unlikely to be perfectly constant across all samples, the "corrected" XPS values may conversely underestimate the actual amine content.

In the case of SiAl+APTES_22.5, both XPS-derived values are significantly lower than the theoretical one, suggesting that at high APTES loadings not all the functionalizing agent is effectively included in the material, resulting in a lower-than-expected amine content.

All samples are amorphous (Fig. 5A), coherently with what expected for silica-based aerogels [46,45].

According to the nitrogen adsorption isotherms (Fig. 6A), all samples are mesoporous, with elevated specific surface area (between 530 m^2/g and 880 m^2/g), high pore volume (between 1.2 cm^3/g and 3.0 cm^3/g) and pores sizing mainly between 10 nm and 20 nm (Fig. 6B). A decrease in textural properties is observed in the sample with the highest APTES content. A clear explanation of this trend would require further investigation, which is out of scope of the present work. However, it may be speculated that, when APTES is added during the one-pot functionalization, some amino groups are confined inside the silica network, while others are exposed inside the silica pores. When the amount of APTES is high, amino-groups are more likely to be exposed inside the pores, which results in a decrease of the surface area and pore volume values. For all samples the apparent density is equal or lower than 0.30 g/cm^3 (Table 4), confirming that the materials are highly porous. All these characteristics are coherent with those of aerogels apt to adsorb CO_2.

In the samples functionalized with APTES, the presence of organic components (Fig. 2) can be attributable both to the alkyl chain of APTES and to the incomplete hydrolysis of the precursors. However, an unquestionable proof of the APTES incorporation is provided by the presence of amino groups, as observed by FTIR (Fig. 2) and XPS analyses (Fig. 3A). Interestingly, in the samples with the lowest APTES content (SiAl+APTES_2.5 and SiAl+APTES_7.5), N is mainly present in protonated form (which is unsuitable to interact with CO_2), while in the sample with the highest APTES content (SiAl+APTES_22.5) N is mainly detected in deprotonated form, which is able to interact with CO_2. This difference may justify the diverse behaviour of the samples in terms of CO_2 adsorption. At this stage, only hypotheses can be done on the source of protonation. Simulations reported in the literature suggest that amino groups of APTES grafted on silica could interact with free silanols through H bonds [47]. If this hypothesis is correct, the source of protonation (i.e.: the silanols) is limited and it may be completely "consumed" when a sufficient amount of APTES is added. Therefore, any further addition of APTES cannot be protonated, justifying the presence of deprotonated N in the sample with the highest APTES content.

Indeed, as far as CO_2 adsorption is concerned, negligible differences are observed in the total adsorbed amount between SiAl, SiAl+APTES_2.5, and SiAl+APTES_7.5 (Fig. 8), suggesting that functionalization with a low number of amino groups does not confer a discernible advantage at elevated partial pressures. However, the initial concavity of the curve of SiAl+APTES_7.5 reveals some affinity between the adsorbate and the surface; indeed, at low pressure this sample adsorbs more CO_2 with respect to the other samples at equivalent partial pressures. A significantly higher adsorption capacity (both total and at low pressure) is observed for the SiAl+APTES_22.5 sample (Fig. 8). This is confirmed by the *in situ* FTIR results (Fig. 9): on SiAl and SiAl+APTES_2.5 samples only molecular CO_2 is observed, indicating that pure physisorption takes place. Instead, on SiAl+APTES_7.5 and, even more, on SiAl+APTES_22.5 new bands due to the presence of carbamates appear even at low CO_2 pressure. This is a sign that CO_2 interacts with these sorbents first and mainly through chemisorption. Taking into consideration XPS (Fig. 3A) and *in situ* FTIR results (Fig. 9), it can be hypothesized that in the samples with the lowest amine content the majority of the amino groups is in protonated form and, therefore, not active for CO_2 capture. By increasing the amino content, in addition to the protonated part, non-protonated groups also appear. Precisely these last groups are those responsible for the preferential adsorption of CO_2, which leads to the formation of carbamates. As far as the total adsorption capacity is concerned, it should be underlined that a comparison with the literature is not trivial, because adsorption tests vary between one study and another. In particular, when samples are prepared, different temperatures and different outgas durations are reported. It should be kept in mind that different outgas conditions may have a significant influence on the adsorption results (higher temperatures and/or longer times of outgas may lead to better adsorption behaviour). Nevertheless, SiAl+APTES_22.5 presents a CO_2 adsorption value in line with those reported in the literature for similar systems.

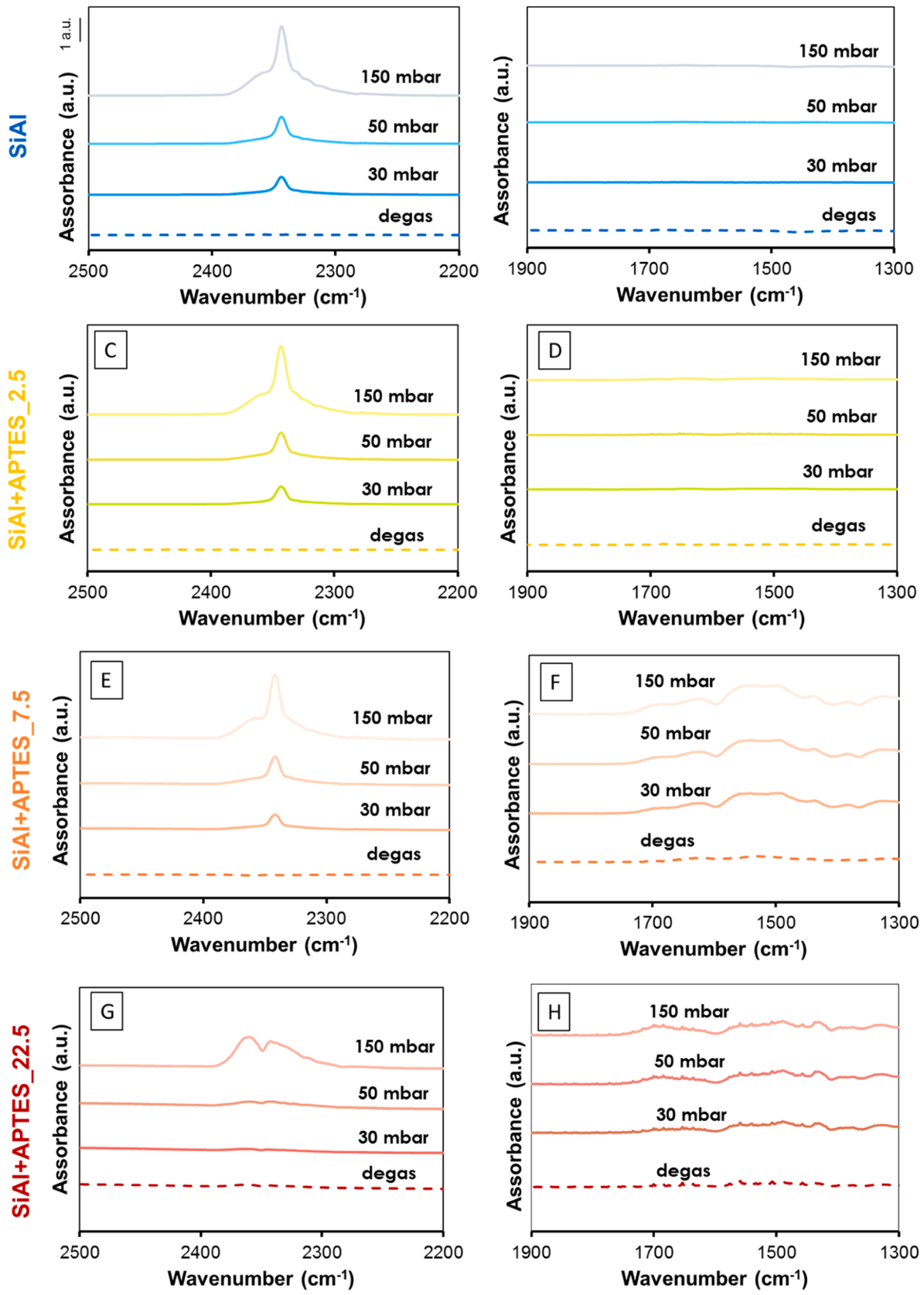

Fig. 9. In situ FTIR difference spectra at increasing CO_2 pressures for samples without (SiAl, A-B) and with functionalization (SiAl+APTES, C-D-E-F-G-H).

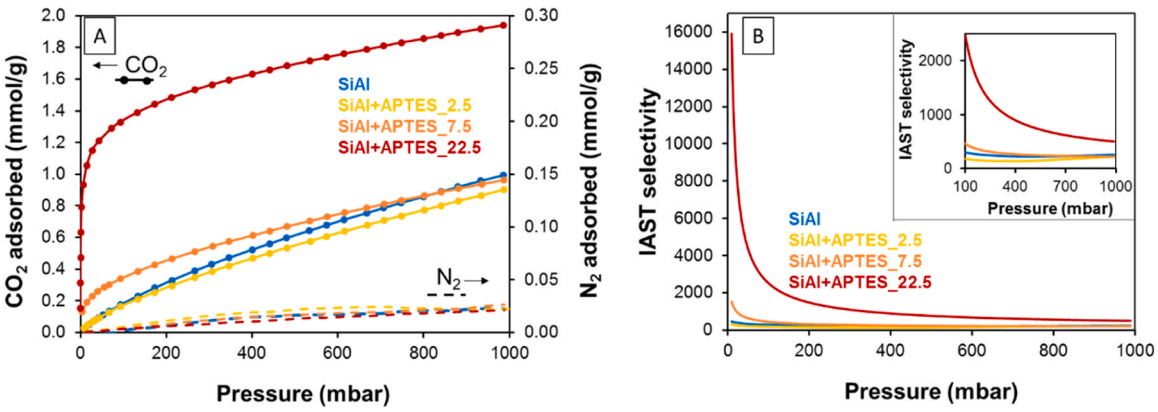

Fig. 10. CO_2 and N_2 adsorption isotherms at 25 °C of the samples (A) and the resulting IAST selectivity on the whole pressure range analysed (B) and in a narrower range (inset in B).

Table 5
Amine content of the functionalized samples according to XPS and theoretical data (mmol of ammine per gram of silica, mmol/g).

Sample	Amine content from XPS (mmol/g)	Amine content from XPS "corrected" (mmol/g)	Theorical amine content (mmol/g)
SiAl+APTES_2.5	2.1	0.8	1.4
SiAl+APTES_7.5	4.7	3.2	4.2
SiAl+APTES_22.5	7.7	6.1	12.5

Indeed, in their work Oliveira and co-authors [48] report the adsorption performance of several silica aerogels or mesoporous silicas functionalized with amino groups: in all cases, the amount of CO_2 adsorbed is around 2 mmol/g. Higher values are obtained only when adsorption tests are performed at high pressure (from 10 bar to 120 bar). Another work, by Choi et al. [9], reports that amine-incorporated silica aerogels can adsorb 3.1 mmol/g of CO_2. However, this value is obtained for a sample with an amine content more than double than those reported in the present study.

The sample with the highest amino content (SiAl+APTES_22.5) also presents the best performance in terms of selectivity (Fig. 10B). The high selectivity is mainly due to the highest affinity with CO_2, both at low and high pressure (Fig. 10A). No relevant differences in selectivity, instead, are observed between the samples with lower CO_2 content and the sample as such. Few selectivity data are available in the literature for similar systems. Nevertheless, when compared to an amine-incorporated silica aerogel with similar amine-content, SiAl+APTES_22.5 presents higher selectivity for a given pressure (e.g., at 400 mbar SiAl+APTES_22.5 has a selectivity of 950, while that reported in the literature is roughly equal to 600 [9]).

To conclude, this explorative work proves the feasibility of a one-pot procedure for synthesizing silica-alumina aerogels functionalized with amino groups. Such an approach guarantees an easy functionalization, efficient in terms of time (it avoids multiple steps) and resources (it does not require the use of additional solvents, heating…), which achieves a uniform distribution of the functional groups. The main disadvantages of the one-pot approach are that not all molecules are appropriate for this procedure and that the synthesis process should be optimized for each functional group. Therefore, to better evaluate the advantages and disadvantages of this technique, it may be useful, in the future, to compare these materials with post-synthesis-functionalized silica-alumina aerogels.

5. Conclusion

Monolithic silica-alumina aerogels functionalized with amino groups have effectively been prepared through a novel one-pot process followed by supercritical CO_2 drying. Different amounts of amino groups were introduced by adding APTES during the sol-gel synthesis of the aerogels. The obtained samples present characteristics, in terms of textural properties and apparent density, which are consistent with those of aerogels and suitable for the capture of CO_2. As suggested by the physico-chemical characterisation and CO_2 adsorption tests, the lowest APTES content does not confer properties significantly different from those of the non-functionalized material. Above a certain threshold, however, the addition of APTES causes an increase in the affinity between the sorbent and CO_2, which interact both through chemi- and physi-sorption. At the highest APTES content, the differences become even more pronounced: not only the affinity increases, but also the total amount of adsorbed CO_2 and the selectivity over N_2. Overall, these results confirm that silica-alumina aerogels functionalized with amino groups are a promising support for CO_2 adsorption in the framework of developing more efficient CO_2 capture technologies.

CRediT authorship contribution statement

Silvia Ronchetti: Writing – review & editing, Validation, Resources, Conceptualization. **Mauro Banchero:** Writing – review & editing, Validation, Supervision, Resources, Methodology, Funding acquisition, Conceptualization. **Fabiana Mangano:** Investigation, Data curation, Conceptualization. **Marta Gallo:** Writing – original draft, Methodology, Investigation, Data curation, Conceptualization. **Marco Armandi:** Writing – review & editing, Validation, Resources, Conceptualization. **Luigi Manna:** Writing – review & editing, Validation, Supervision, Resources, Methodology, Funding acquisition, Conceptualization.

Declaration of Competing Interest

The authors declare that they have no known competing financial interests or personal relationships that could have appeared to influence the work reported in this paper.Appendix ASupporting information

Appendix A. Supporting information

Supplementary data associated with this article can be found in the online version at doi:10.1016/j.supflu.2025.106835.

Data availability

Data will be made available on request.

References

[1] M. Meinshausen, et al., Greenhouse-gas emission targets for limiting global warming to 2°C, Nature 458 (7242) (2009) 1158–1162, https://doi.org/10.1038/nature08017.

[2] L. Keshavarz, M.R. Ghaani, J.M.D. MacElroy, N.J. English, A comprehensive review on the application of aerogels in CO2-adsorption: materials and characterisation, Chem. Eng. J. 412 (2021), https://doi.org/10.1016/j.cej.2021.128604.

[3] L. Du, T. Lu, B. Li, CO2 capture and sequestration in porous media with SiO2 aerogel nanoparticle-stabilized foams, Fuel 324 (2022), https://doi.org/10.1016/j.fuel.2022.124661.

[4] J. Feng, L. Fan, M. Zhang, M. Guo, An efficient amine-modified silica aerogel sorbent for CO2 capture enhancement: facile synthesis, adsorption mechanism and kinetics, Colloids Surf. A Physicochem Eng. Asp. 656 (2023), https://doi.org/10.1016/j.colsurfa.2022.130510.

[5] B. Yay, N. Gizli, A review on silica aerogels for CO2 capture applications, Pamukkale Univ. J. Eng. Sci. 25 (7) (2019) 907–913, https://doi.org/10.5505/pajes.2018.35651.

[6] Z.D. Shao, X. Cheng, Y.M. Zheng, Facile co-precursor sol-gel synthesis of a novel amine-modified silica aerogel for high efficiency carbon dioxide capture, J. Colloid Interface Sci. 530 (2018) 412–423, https://doi.org/10.1016/j.jcis.2018.06.094.

[7] R. Saliger, T. Heinrich, T. Gleissner, J. Fricke, Sintering behaviour of alumina-modified silica aerogels, J. Non-Cryst. Solids 86 (1995) 113–117, https://doi.org/10.1016/0022-3093(95)00080-1.

[8] S. Cui, S. Yu, B. Lin, X. Shen, X. Zhang, D. Gu, Preparation of amine-modified SiO2 aerogel from rice husk ash for CO2 adsorption, J. Porous Mater. 24 (2017) 455–461, https://doi.org/10.1007/s10934-016-0280-2.

[9] H. Choi, H.H. Han, V.G. Parale, T. Kim, W. Park, Y. Kim, J. Kim, Y. Choi, Y.S. Bae, H.H. Park, Rigid amine-incorporated silica aerogel for highly efficient CO2 capture and heavy metal removal, Chem. Eng. J. 483 (2024) 149357, https://doi.org/10.1016/j.cej.2024.149357.

[10] M.E. Potter, K.M. Cho, J.J. Lee, C.W. Jones, Role of alumina basicity in CO2 uptake in 3-aminopropylsilyl-grafted alumina adsorbents, ChemSusChem 10 (2017) 2192–2201, https://doi.org/10.1002/cssc.201700115.

[11] N. Linneen, R. Pfeffer, Y.S. Lin, CO2 adsorption performance for amine grafted particulate silica aerogels, Chem. Eng. J. 254 (2014) 190–197, https://doi.org/10.1016/j.cej.2014.05.087.

[12] N. Linneen, R. Pfeffer, Y.S. Lin, CO2 capture using particulate silica aerogel immobilized with tetraethylenepentamine, Microporous Mesoporous Mater. 176 (2013) 123–131, https://doi.org/10.1016/j.micromeso.2013.02.052.

[13] J. Feng, L. Fan, M. Zhang, M. Guo, An efficient amine-modified silica aerogel sorbent for CO2 capture enhancement: facile synthesis, adsorption mechanism and kinetics, Colloids Surf. A Physicochem. Eng. Asp. 656 (2023) 130510, https://doi.org/10.1016/j.colsurfa.2022.130510.

[14] H. Tamon, T. Sone, M. Mikami, M. Okazaki, Preparation and characterization of silica-titania and silica-alumina aerogels, J. Colloid Interface Sci. 188 (2) (1997) 493–500, https://doi.org/10.1006/jcis.1997.4779.

[15] M. Castiglioni, L. Rivoira, M. Gallo, I. Ingrando, M. Del Bubba, B. Onida, M. C. Bruzzoniti, Removal of sugars from food and beverage wastewaters by amino-modified SBA-15, J. Clean. Prod. 324 (2021) 129236, https://doi.org/10.1016/j.jclepro.2021.129236.

[16] S. Brunauer, P.H. Emmett, E. Teller, Adsorption of gases in multimolecular layers, J. Am. Chem. Soc. 60 (1938) 309–319, https://doi.org/10.1021/ja01269a023.

[17] E.P. Barrett, L.G. Joyner, P.P. Halenda, The determination of pore volume and area distributions in porous substances". I. Computations from nitrogen isotherms, J. Am. Chem. Soc. 73 (1951) 373–380, https://doi.org/10.1021/ja01145a126.

[18] A.L. Myers, J.M. Prausnitz, Thermodynamics of mixed-gas adsorption, AIChE J. 11 (1965) 121–127, https://doi.org/10.1002/aic.690110125.

[19] M. Ismail, M.A. Bustam, N.E.Fatriyah Kari, Y.F. Yeong, Ideal adsorbed solution theory (IAST) of carbon dioxide and methane adsorption using magnesium gallate metal-organic framework (Mg-gallate), Molecules 28 (2023) 3016, https://doi.org/10.3390/molecules28073016.

[20] A.L. Myers, J.M. Prausnitz, Thermodynamics of mixed-gas adsorption, AIChE J. 11 (1) (1965) 121–127, https://doi.org/10.1002/aic.690110125.

[21] B. Szczęsniak, J. Choma, Graphene-containing microporous composites for selective CO2 adsorption, Microporous Mesoporous Mater. 292 (2020) 109761, https://doi.org/10.1016/j.micromeso.2019.109761.

[22] E. Davarpanah, M. Armandi, S. Hernández, D. Fino, R. Arletti, S. Bensaid, M. Piumetti, CO_2 capture on natural zeolite clinoptilolite: effect of temperature and role of the adsorption sites, J. Environ. Manag. 275 (2020) 111229, https://doi.org/10.1016/j.jenvman.2020.111229.

[23] J.L.R. Silveira, S.R. Dib, A.M. Faria, New support for high-performance liquid chromatography based on silica coated with alumina particles, Anal. Sci. 30 (2) (2014) 285–291, https://doi.org/10.2116/analsci.30.285.

[24] G. Socrates, 2001, Infrared and Raman Characteristic Group Frequencies: Tables and Charts.

[25] W.T. Al-Rubayee, O.F. Abdul-Rasheed, N.M. Ali, Preparation of a modified nanoalumina sorbent for the removal of Alizarin Yellow R and Methylene Blue dyes from aqueous solutions, J. Chem. (2016), https://doi.org/10.1155/2016/4683859.

[26] D. Lin-Vien, N.B. Colthup, W.G. Fateley, J.G. Grasselli, Chapter 10 - Compounds containing –NH2, –NHR, and –NR2 Groups", from, Handb. Infrared Raman Charact. Freq. Org. Mol. (1991) 155–178, https://doi.org/10.1016/B978-0-08-057116-4.50016-X.

[27] J. Shen, Y.N. Wu, B. Zhang, F. Li, Preparation of mesoporous silica nanosheets through electrospinning: A novel scroll mechanism, RSC Adv. 4 (25) (2014) 12805–12808, https://doi.org/10.1039/c3ra47504b.

[28] W. Zhu, Y. Yao, Y. Zhang, H. Jiang, Z. Wang, W. Chen, Y. Xue, Preparation of an amine-modified cellulose nanocrystal aerogel by chemical vapor deposition and its application in CO2 capture, Ind. Eng. Chem. Res. 59 (38) (2020) 16660–16668, https://doi.org/10.1021/acs.iecr.0c02687.

[29] D. Brunel, A.C. Blanc, E. Garrone, B. Onida, M. Rocchia, J.B. Nagy, D. J. Macquarrie, Spectroscopic studies on aminopropyl-containing micelle templated silicas. Comparison of grafted and co-condensation routes, Stud. Surf. Sci. Catal. 142 (2002) 1395–1402, https://doi.org/10.1016/S0167-2991(02)80305-6.

[30] N.M. Figueiredo, N.J.M. Carvalho, A. Cavaleiro, An XPS study of Au alloyed Al-O sputtered coatings, Appl. Surf. Sci. 257 (13) (2011) 5793–5798, https://doi.org/10.1016/j.apsusc.2011.01.104.

[31] A.G. Shard, B.P. Reed, D.J.H. Cant, Surface analysis insight note: uncertainties in XPS elemental quantification, Surf. Interface Anal. 57 (6) (2025) 389–395, https://doi.org/10.1002/sia.7398.

[32] C. Verma, M.A. Quraishi, K.Y. Rhee, Hydrophilicity and hydrophobicity consideration of organic surfactant compounds: effect of alkyl chain length on corrosion protection, Adv. Colloid Interface Sci. 306 (2022) 102723 doi10.1016/j.cis.2022.102723.

[33] H.E. Bergna. "The Colloid Chemistry of Silica". Comstock, J., Ed., Advances in Chemistry Series. 1994. 234. American Chemical Society, Washington DC. doi:10.1021/ba-1994-0234.

[34] K. Pielichowski, T.M. Majka, Polymer Composites with Functionalized Nanoparticles, Elsevier, 2019, https://doi.org/10.1016/C2017-0-00517-7.

[35] E.J. Cueto-Díaz, A. Castro-Muñiz, F. Suárez-García, S. Gálvez-Martínez, M. C. Torquemada-Vico, M.P. Valles-González, E. Mateo-Martí, APTES-Based Silica Nanoparticles as a Potential Modifier for the Selective Sequestration of CO_2 Gas Molecules, Nanomaterials 11 (2021) 2893, https://doi.org/10.3390/nano11112893.

[36] M. Gallo, L. Serpella, F. Leone, L. Manna, M. Banchero, S. Ronchetti, B. Onida, Piroxicam loading onto mesoporous silicas by supercritical CO2 impregnation, Molecules 26 (2021) 2500, https://doi.org/10.3390/molecules26092500.

[37] M. Gallo, F. Giudice, M. Banchero, S. Ronchetti, L. Manna, B. Onida, A mesostructured hybrid CTA–silica carrier for curcumin delivery, J. Sol. Gel Sci. Technol. 96 (2020) 236–246, https://doi.org/10.1007/s10971-020-05374-0.

[38] M. Thommes, K. Kaneko, A.V. Neimark, J.P. Olivier, F. Rodriguez-Reinoso, J. Rouquerol, K.S.W. Sing, Physisorption of gases, with special reference to the evaluation of surface area and pore size distribution (IUPAC Technical Report), Pure Appl. Chem. 87 (2015) 1051–1069, https://doi.org/10.1515/pac-2014-1117.

[39] S. Brunauer, P.H. Emmett, E. Teller, Adsorption of gases in multimolecular layers, J. Am. Chem. Soc. 60 (1938) 309–319, https://doi.org/10.1021/ja01269a023.

[40] M. Pavani, 2013, Organosilici a mesoporosità controllata per la cattura e la conversione dell'anidride carbonica". MS Thesis. Politecnico di Torino.

[41] A. Danon, P.C. Stair, E. Weitz, FTIR study of CO2 adsorption on amine-grafted SBA-15: elucidation of adsorbed species, J. Phys. Chem. C 115 (23) (2011) 11540–11549, https://doi.org/10.1021/jp200914v.

[42] C. Knofel, C. Martin, V. Hornebecq, P. Llewellyn, Study of carbon dioxide adsorption on mesoporous aminopropylsilane-functionalized Silica and Titania combining microcalorimetry and in situ infrared spectroscopy, J. Phys. Chem. C 113 (2009) 21726–21734, https://doi.org/10.1021/jp907054h.

[43] M. Gallo, S. Ronchetti, B. Onida, L. Manna, The impregnation of mesoporous silica with diaminohexane by means of supercritical CO_2: a possible CO_2 solid sorbent, J. CO2 Util. 101 (2025) 103207, https://doi.org/10.1016/j.jcou.2025.103207.

[44] M. Etzi, E. Sartoretti, S. Bensaid, M. Allione, S. Ferraris, M. Castellin, M. Armandi, Tuning microporosity and surface chemistry: the synergistic effect of KOH and urea on CO_2 capture performance of sucrose-derived activated carbons, Chem. Eng. J. 521 (2025) 167166, https://doi.org/10.1016/j.cej.2025.167166.

[45] G. Greczynski, L. Hultman, The same chemical state of carbon gives rise to two peaks in X-ray photoelectron spectroscopy, Sci. Rep. 11 (2021) 11195, https://doi.org/10.1038/s41598-021-90780-9.

[46] M. Gallo, B. Onida, L. Manna, M. Banchero, Silica–Cyclodextrin hybrid materials: two possible synthesis processes, Int. J. Mol. Sci. 25 (2024) 1108, https://doi.org/10.3390/ijms25021108.

[47] A.L. Doadrio, J.M. Sánchez-Montero, J.C. Doadrio, A.J. Salinas, M. Vallet-Regí, A molecular model to explain the controlled release from SBA-15 functionalized with APTES, Microporous Mesoporous Mater. 195 (2014) 43–49, https://doi.org/10.1016/j.micromeso.2014.04.019.

[48] R.J. Oliveira, J.F. de Conto, M.R. Oliveira, S.M.S. Egues, G.R. Borges, C. Dariva, E. Franceschi, CO_2/CH_4 adsorption at high-pressure using silica-APTES aerogel as adsorbent and near infrared as a monitoring technique, J. CO2 Util. 32 (2019) 232–240, https://doi.org/10.1016/j.jcou.2019.04.019.